Biophysical Journal, Volume 97

Supporting Material

Specific Membrane Binding of Neurotoxin II Can Facilitate its Delivery to Acetylcholine Receptor

Dmitry M. Lesovoy, Eduard V. Bocharov, Ekaterina N. Lyukmanova, Yurij A. Kosinsky, Mikhail A. Shulepko, Dmitry A. Dolgikh, Mikhail P. Kirpichnikov, Roman G. Efremov, and Alexander S. Arseniev

Supporting Material

Specific Membrane Binding of Neurotoxin II Can Facilitate its Delivery to Acetylcholine Receptor.

Dmitry M. Lesovoy, Eduard V. Bocharov, Ekaterina N. Lyukmanova, Yurij A. Kosinsky, Mikhail A. Shulepko, Dmitry A. Dolgikh, Mikhail P. Kirpichnikov, Roman G. Efremov, and Alexander S. Arseniev

1 NTII retains its overall structure upon membrane binding and amino acid substitutions

NTII possesses "three-finger" β-structural fold, stabilized by four disulfide bonds, which retains its structure up to ~80^{o}C (1). NMR relaxation data (unpublished) also confirm high rigidity of NTII molecule. Stability of the NTII spatial structure upon amino-acid replacements E2Q/D57N was shown by means of solution NMR and CD spectroscopy (supplemental Figs. S2*B* and S4).

To make sure that the binding of NTII to the membrane does not affect its spatial structure, CD spectra of NTII were measured in aqueous solution and in the presence of lipid bilayer (DOPC/DOPS/Chol=3:1:1) (Fig. S2 *A*). These spectra revealed identity of the toxin spatial structures in free-solution and membrane-bound (Lipid/NTII ≥ 40) states. The preservation of NTII spatial structure in a medium mimicking water-membrane interface was also proved by ^{1}H-^{15}N HSQC spectra (supplemental Figs. S3 and S6 and discussion below). So, the NTII spatial structure does not undergo significant changes upon membrane binding.

2 Protein/lipid system construction for MD calculations

Protein and anionic DOPS bilayer (pre-equilibrated as described in (2) were placed into rectangular box of SPC (simple point charge model) waters molecules (3) and 124 Na^{+} ions to render the system electrically neutral. Simulations were carried out with a time step of 2 fs, with imposed 3D periodic boundary conditions. Van der Waals interactions were truncated by use of the twin-range 12/20 Å cutoff function. Electrostatic interactions were treated with the PME (particle mesh Ewald) algorithm (4). All components of the systems were coupled separately to the Berendsen thermostat (5) with a coupling constant of 0.1 ps. Before MD simulations, energy of the system was minimized using 300 steepest descent iterations with fixed protein atoms followed by 300 conjugate gradients steps with fixed backbone, and final relaxation (300 conjugate gradients steps) without constraints. Finally, it was heated from 5 to 300 K during 60 ps in the NVT ensemble followed by 6 ns of unrestrained NPT MD collection run at 300 K.

3 Amplitude reduction effect as a result of chemical shift difference between solution and membrane-bound states of NTII

The experimental line shapes in ^{1}H-^{15}N HSQC spectrum of NTII being in exchange between free-solution and membrane-bound states are determined by a number of factors including the fraction of the membrane bound state, the effective correlation time of the observed nuclei, the exchange rate between these states, and the chemical shift difference of ^{1}H and ^{15}N resonances in free and bound states. So, the precise theoretical interpretation is quite complicated. But the interpretation of differential amplitude reduction of ^{1}H-^{15}N cross-peaks in HSQC spectra was proposed (6) and successfully used for the mapping of binding site of a small protein in complex with a large protein (6,7). Under assumption that ^{1}H dimension gives greatest

contribution to the changes of cross-peak amplitudes, the line shape, $I(\omega)$, of $^1H^N$ of NTII under exchange between solution and membrane-bound states could be described (2) as:

$$I(\omega) =$$
$$[(-\omega+\omega_1-2a\omega_1)\{-2k\omega-(R_f+R_b)\omega+(-R_f+R_b)\omega_1\}+$$
$$\{2k+(1-a)R_f+aR_b\}(R_fR_b+k(R_f+R_b)-\omega^2+\omega_1{}^2)]/$$
$$[\{-2k\omega-(R_f+R_b)\omega+(-R_f+R_b)\omega_1\}^2+$$
$$\{R_fR_b+k(R_f+R_b)-\omega^2+\omega_1{}^2\}^2],$$

where k is the exchange rate between free and bound states in s^{-1}, R_f and R_b are the transverse relaxation rates in s^{-1} of $^1H^N$ nuclei of NTII in solution and membrane-bound states, respectively, $2\omega_1$ is the chemical shifts difference in Hz of $^1H^N$ nuclei between these states, (a) and (1-a) are the probabilities of occurrence for the free and bound states, respectively. In the aqueous solution, $^1H^N$ nuclei of NTII possess R_f ~10 s^{-1} (estimated from linewidth in 1D ^1H NMR spectra). In the state fully bound to membranes, ^1H NMR signals of NTII are broadened beyond detection, so R_b>>10 s^{-1}. Upper bound of R_b could be estimated under an assumption that NTII molecule is strongly associated with lipid bilayer and rotates as a whole with 1000 Å liposomes, corresponding to rotational correlation time ~10^{-4} s (according to Stokes' law), which results in approximately R_b~10^5 s^{-1} (8). Chemical shift difference between solution and membrane-bound states could be assumed to be not large as for cytotoxins, i.e. up to ~300 Hz (chemical shift difference between solution and dodecylphosphocholine (DPC) micelle bound state for $^1H^N$ nuclei from DPC bound site of cytotoxin)(9). In the case of slow and intermediate (in the NMR time scale) exchange rate k<<≈300 s^{-1}, the NTII $^1H^N$ signals undergo the differential amplitude reduction (6). Dependence of the amplitude reduction on chemical shift difference of $^1H^N$ nuclei between solution and membrane-bound states of NTII was simulated for a=0.5 (supplemental Table S1). Corresponding experimental ^1H-^{15}N HSQC spectra display differential amplitude reduction in about 40-50% (Fig. 2 *A*, *B*). Also, the experimental ^1H-^{15}N HSQC spectra of NTII partially bound to membrane do not undergo noticeable chemical shift changes in comparison with NTII in aqueous solution. So, comparison of the experimental and simulated spectra with variation of R_b and k values (supplemental Table S1) shows that the experimental spectra correspond to R_b~10^2 s^{-1} and exchange rate k~10^2 s^{-1}. It is interesting to note that the estimated value of R_b~10^2 s^{-1} implies that NTII diffuses not as a whole with liposome (corresponding R_b~10^5 s^{-1}) but undergoes essential lateral diffusion and tumbling on the liposome surface. These effective motions are about 10 times slower then the tumbling of NTII in aqueous solution.

4 NTII NMR signal perturbations in response to environment properties

In order to take into account possible hypersensitivity of chemical shifts of $^1H^{15}N$ cross-peaks of Glu2, Cys3, Gln6, Cys17, Gly41, Asn50, and Arg58 residues (undergoing differential amplitude reduction upon NTII membrane binding Fig. 2) to changes of environment conditions near the liposome surface, several ^1H-^{15}N HSQC spectra for NTII in different solutions mimicking the possible medium changes were obtained. In this way, an influence of decreases of dielectric constant and pH as well as ion concentration increase near the anionic membrane surface (10, 11) were assayed. It is known that upon transition from bulk water to anionic lipid bilayer surface, dielectric constant changes from 80 to ~40 and could be simulated by varying methanol/water ratio from 0% to 60% (10).

Upon variations of the methanol/water ratio, pH, and KCl concentration, the combined $^1H^{15}N$ (^1H and ^{15}N) chemical shift changes in ^1H-^{15}N HSQC spectra of NTII (Fig. S6) and

changes of cross-peak amplitudes of backbone and side chains of Glu2, Cys3, Cys17, Gly41, and Arg58 residues were close to the average values along the sequence of NTII. However, variation of the chemical shifts (Fig. S6 *B*) of side chain NH2 group of Asn50 reveals their prominent sensitivity to dielectric constant. Thus, this residue can not serve as an unambiguous probe of NTII topology on the membrane surface.

Unlike dielectric constant, the variation of pH and KCl concentration has smaller effect on the combined $^{1}H^{15}N$ chemical shift values (Fig. S6**)**. The variation of KCl concentration in the range from 75 mM (corresponding to bulk KCl concentration where the differential amplitude reduction was analyzed, Fig. 2 *A*, *B*) to 240 mM revealed significant sensitivity of backbone NH of Glu20 and side chain NH2 group of Asn22 to the salt concentration in the sample (Fig. S6 *C*, *D*). Probably, this indicates the presence of a cation binding site near Glu20 and Asn22 residues. The variation of pH from 5.5 (bulk pH in membrane binding experiments) to 5.0 (simulation of pH reduction near anionic membrane surface (10)), showed significant sensitivity of NH2 cross-peaks of Gln6 side chain (Fig. S6 *F*). Taking into account the pKa values of 5.0 and 5.8 for His4 and His31, respectively, and that pKa values of other ionizable groups in NTII are less then 3.8 (unpublished data), this observation can be explained by spatial proximity of Gln6 side chain to imidazole ring of His4.

To sum up, our experimental data indicate that the disposition of NTII near the membrane surface can influence the chemical shifts of NH and NH2 signals of Gln6, Asn22, and Asn50 residues without their direct interaction with membrane. However, the location of Gln6 and Asn22 in close proximity to the proposed DOPS binding site (Fig. 2, Fig. 3) explains the observed differential amplitude reduction for cross-peaks of these residues too (Fig. 2). These observations favor mapping the membrane binding site in the head region of NTII.

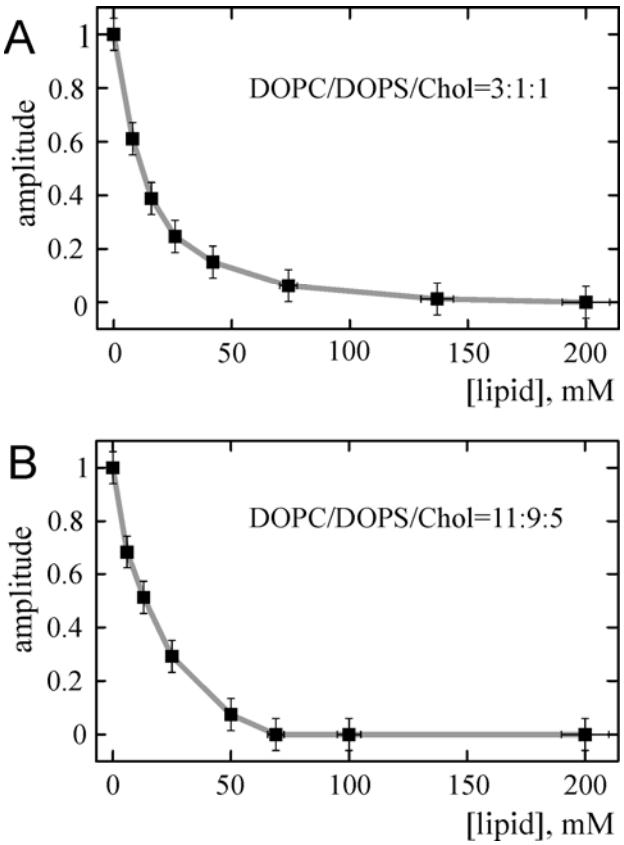

FIGURE S1 Neurotoxin II binding to native-like nAChR membrane at physiological ionic strength as a function of lipid concentration. Average amplitude of ^{1}H-NMR signals of 1 mM NTII in the presence of the membrane at different lipid concentration were normalized to the corresponding values for the free solution state of NTII. The ^{1}H-NMR spectra were obtained at ~150 mM ionic strength (including 50 mM NaOAc buffer and total 100 mM salt concentration), pH 5.5, 303 K.

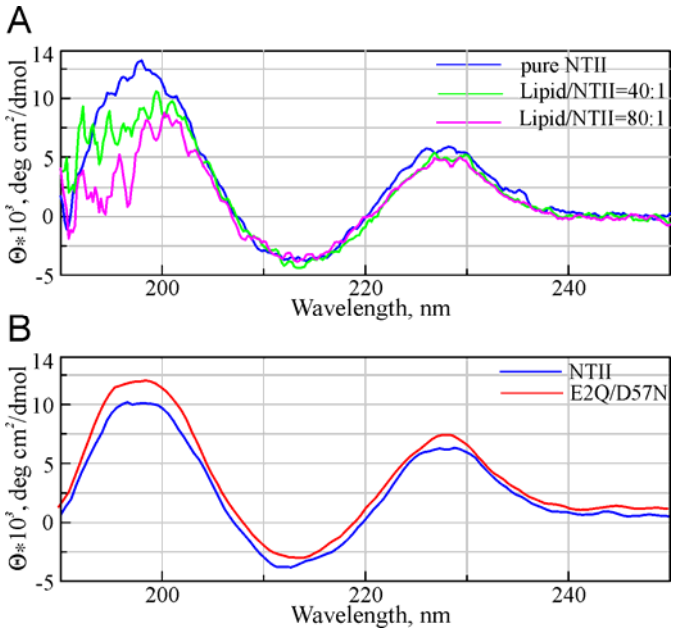

FIGURE S2 CD monitoring of NTII structure upon the membrane binding and amino acid substitutions. (***A***) CD spectra of NTII in aqueous solution and in lipid bilayer (full binding to monolamellar DOPC/DOPS/Chol=3:1:1 liposomes). The observed lack of coincidence in the far-UV region (190-200nm) of the spectra was due to light-scattering on liposomes. (***B***) CD spectra of NTII and $NTII_{E2Q/D57N}$ in aqueous solution. All the spectra were measured at 30°C in 30 mM KCl, 10 mM NaOAc, pH 5.5.

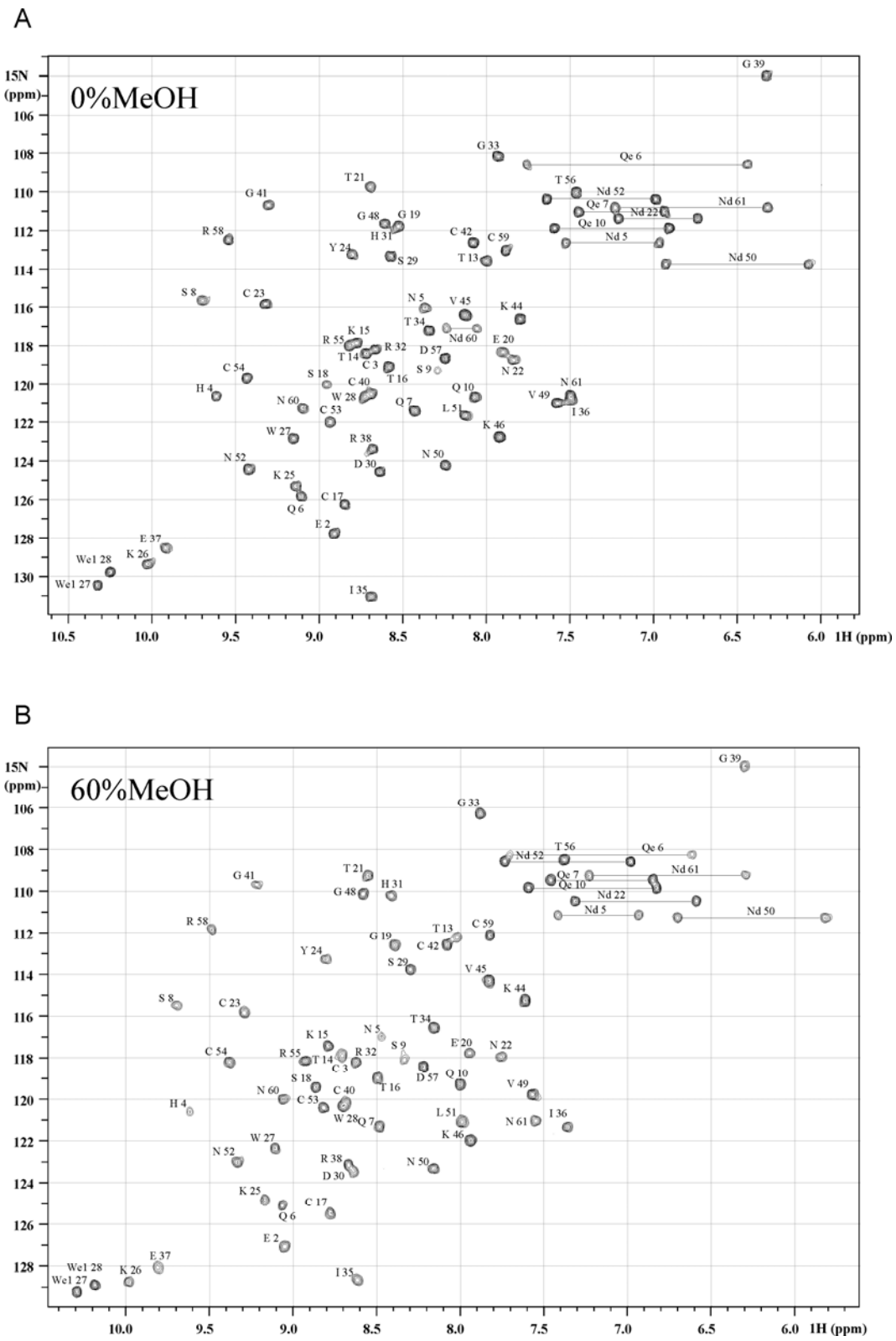

FIGURE S3 ^{1}H-^{15}N HSQC spectra of NTII in aqueous solution (*A*) and in 60% methanol (*B*). The spectra were measured at 303^{o}K in 10 mM NaOAc, pH 5.5. The ^{1}H-^{15}N backbone and side chain resonance assignments are shown.

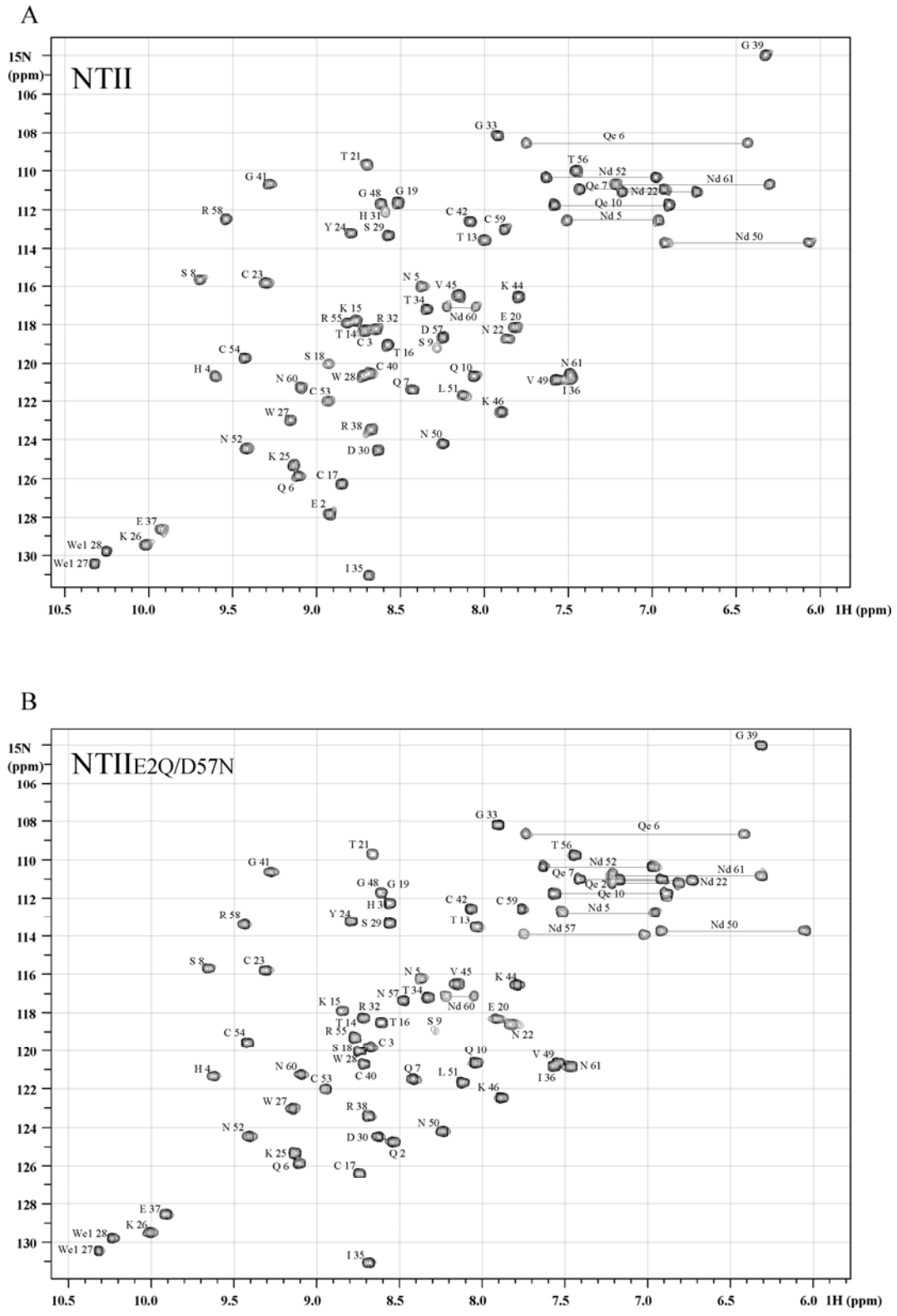

FIGURE S4 ^{1}H-^{15}N HSQC spectra of NTII (*A*) and its E2Q/D57N mutant form (*B*) in aqueous solution. The spectra were measured at 30^{o}C in 10 mM NaOAc, pH 5.5. The ^{1}H-^{15}N backbone and side chain resonance assignments are shown. The values of NTII and $NTII_{E2QD57N}$ masses as determined by MALDI-MS (6877 and 6876, respectively) were identical to theoretical ones adjusted for method error (1 Da).

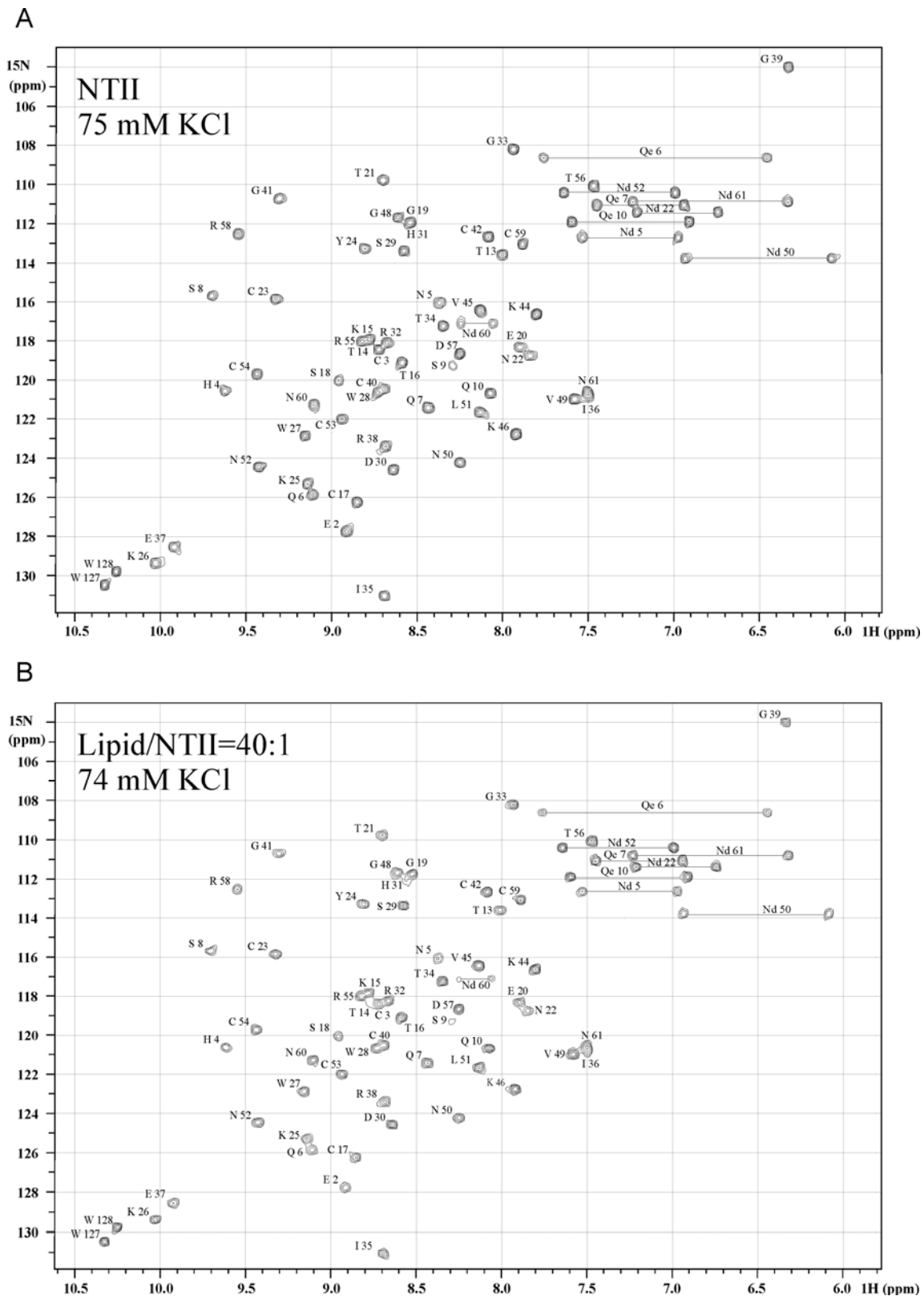

FIGURE S5 ^{1}H-^{15}N HSQC spectra of (*A*) NTII in aqueous solution and (*B*) NTII in aqueous suspension of monolamellar DOPC/DOPS/Chol = 3:1:1 liposomes (Lipid/NTII = 40:1). The spectra were measured at 30^{o}C in 10 mM NaOAc, pH 5.5 and ~75 mM KCl. The ^{1}H-^{15}N backbone and side chain resonance assignments are shown.

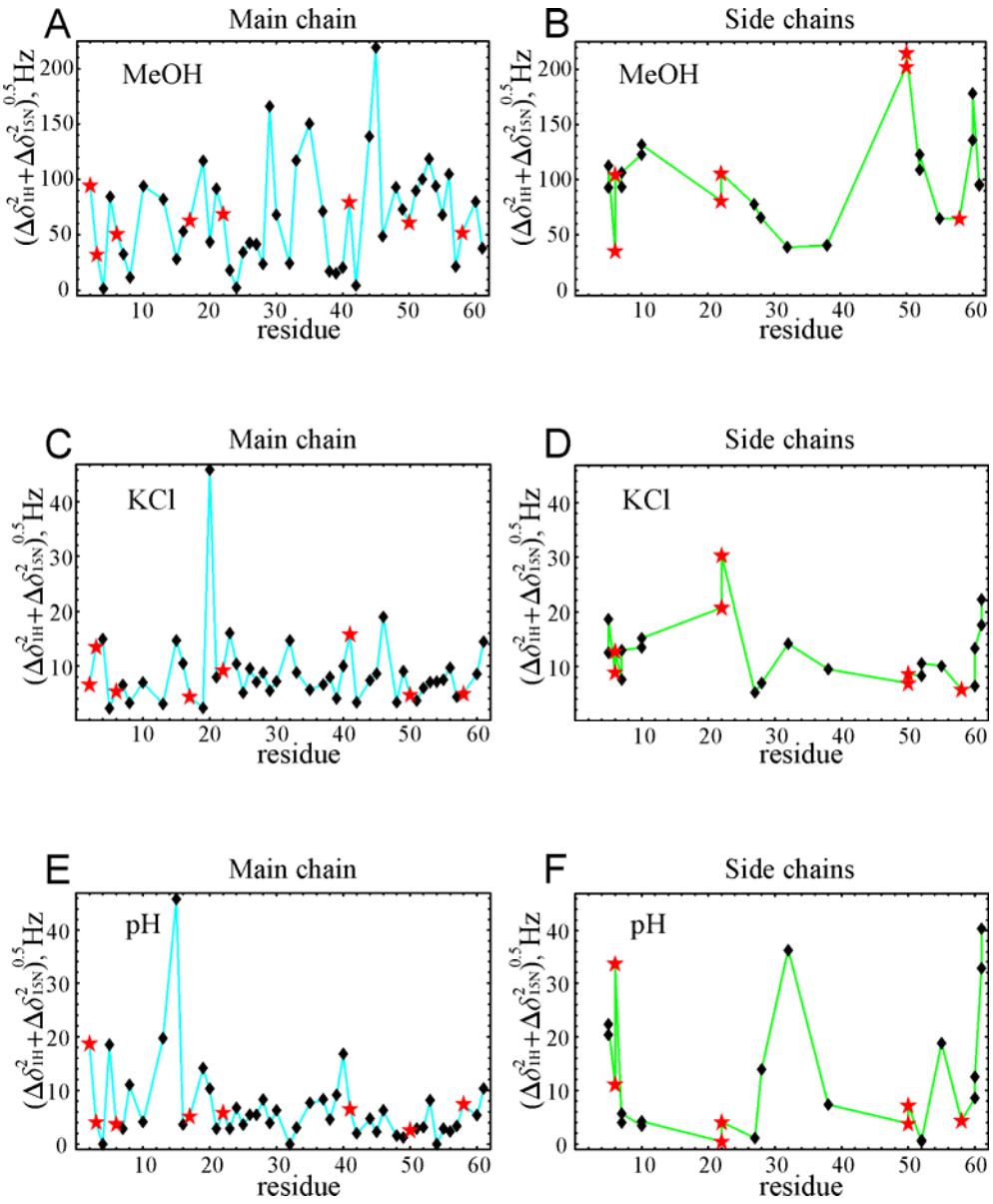

FIGURE S6 Sensitivity of $^{1}H^{15}N$ chemical shifts of NTII to changes of environment properties. The variations in ^{1}H and ^{15}N combined chemical shifts for NH and NH2 groups in ^{1}H-^{15}N HSQC spectra of 0.4 mM NTII in aqueous solution at 30^{o}C, 10 mM NaOAc, pH 5.5 (if not otherwise specified) are shown. The combined chemical shifts changes in response to changes of (***A***, ***B***) methanol concentration (from 0% to 60%), (***C***, ***D***) KCl concentration (from 75 to 250 mM) and (***E***, ***F***) pH value (from pH 5.5 to 5.0). Chemical shift changes of $^{1}H^{15}N$ cross-peaks of the Glu2, Cys3, Gln6, Cys17, Asn22, Gly41, Asn50, and Arg58 residues (undergoing amplitude reduction effect upon membrane binding **Fig. 2**) are denoted by red asterisks.

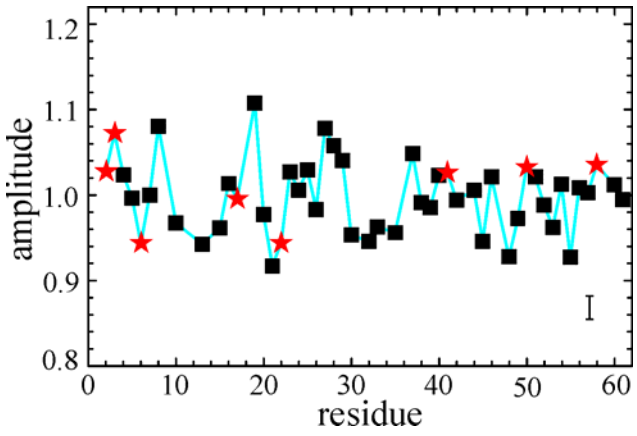

FIGURE S7 Sensitivity of $^{1}H^{15}N$ cross-peak amplitudes in ^{1}H-^{15}N HSQC spectra of NTII to KCl concentration. The $^{1}H^{15}N$ cross-peak amplitudes of backbone NH groups of 0.4 mM NTII 10 mM NaOAc, in aqueous solution at pH 5.5, 30^{o}C. The ratios of the cross-peak amplitudes at 75 mM KCl and at 240 mM KCl are plotted against NTII residue number (as on **Fig. 2** ***B***). The residues Glu2, Cys3, Gln6, Cys17, Asn22, Gly41, Asn50, and Arg58 (undergoing amplitude reduction effect upon membrane binding **Fig. 2**) are marked by red asterisks. The experimental error is shown by bar in the right corner of the diagram.

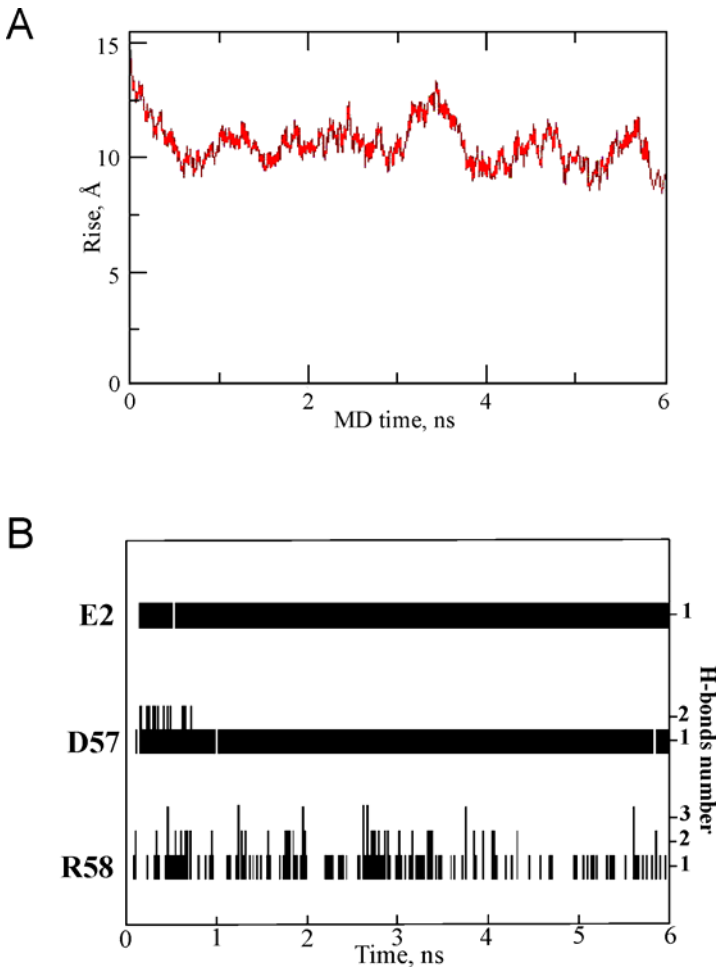

FIGURE S8 Results of MD simulations of NTII/membrane interaction. ***A*****,** Time course of z-coordinate (rise) of the center of mass of NTII with respect to the DOPS bilayer surface (defined as average position of phosphorous atoms of lipids in the nearest monolayer). ***B*****,** The number of hydrogen bonds formed between the most stably bound DOPS molecule of the implicit lipid membrane and Glu2, Asp57 and Arg58 residues of NTII. The data are presented as diagrams, where the height of a bar corresponds to 1, 2 or 3 hydrogen bonds per corresponding side chain of NTII.

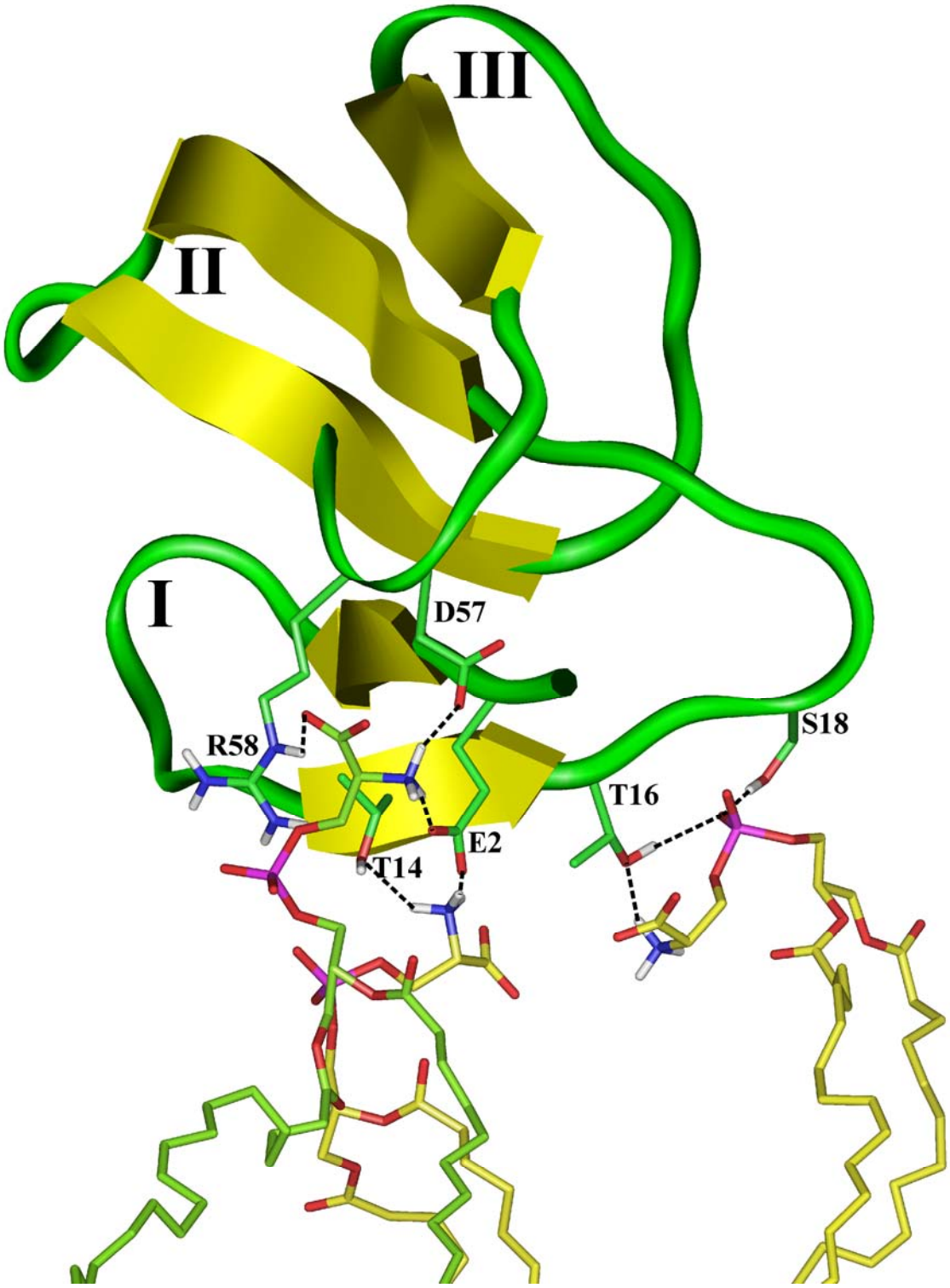

FIGURE S9 Intermolecular hydrogen bonds between NTII and DOPS molecules identified by MD simulation. NTII forms the most stable contact with one DOPS molecule (shown in green) through Glu2, Asp57, and Arg58 residues. Also, the toxin interacts occasionally with additional two DOPS molecules (shown in yellow) by Glu2, Thr14, Thr16, and Ser18 residues. The intermolecular hydrogen bonds are shown with dashed lines.

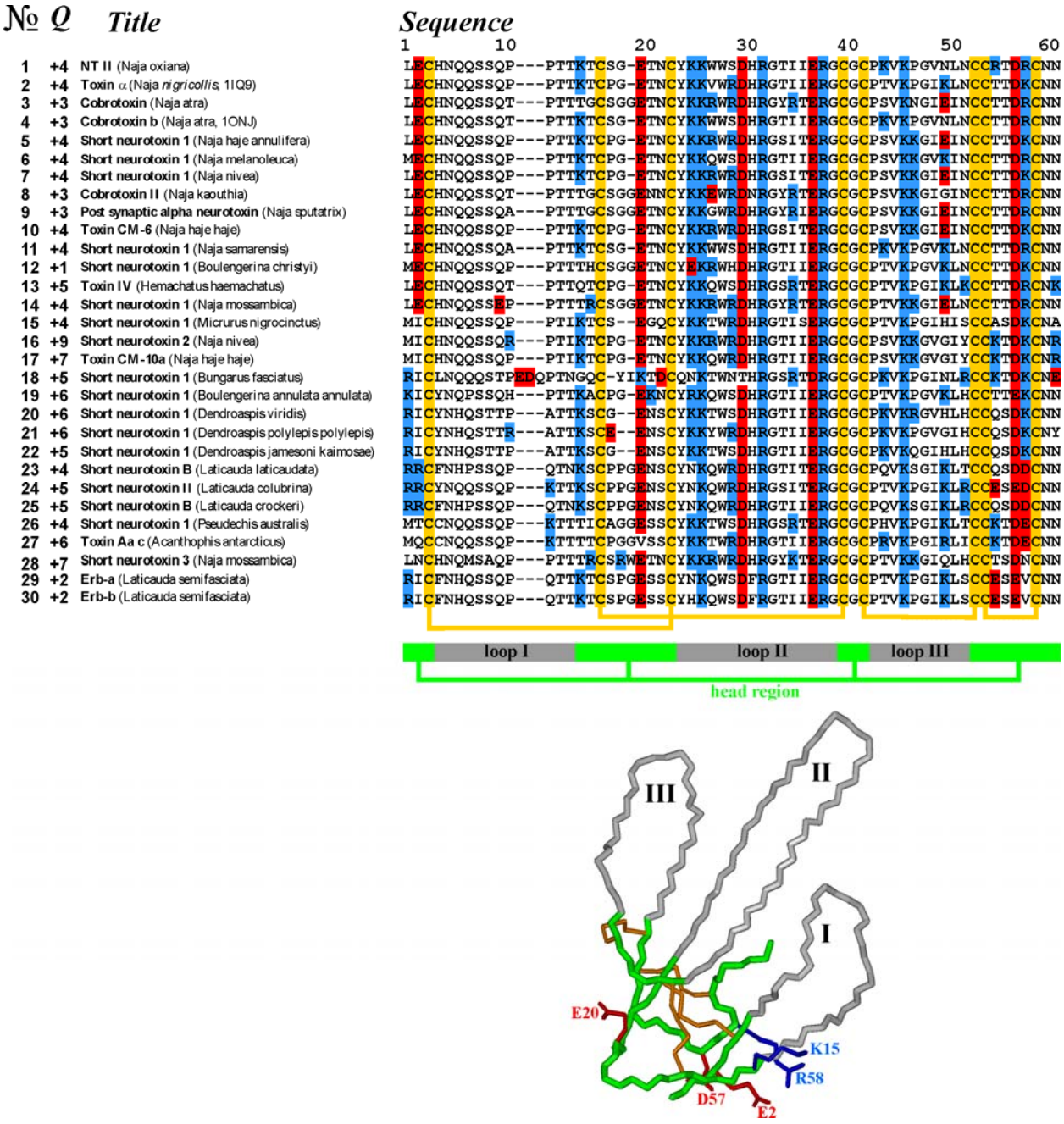

FIGURE S10 Sequence homology of short-chain α-neurotoxins. The residue numbers are shown above the sequences and correspond to NTII. The toxins total charges Q are indicated for physiological pH 7.0. Cys residues, the residues with negatively (Asp and Glu) and positively (Arg and Lys) charged side chains are highlighted in *yellow*, *red,* and *blue*, respectively. At the bottom the structural elements S-S bonds, loops and head region of NTII are displayed in orange lines, green and gray boxes, respectively.

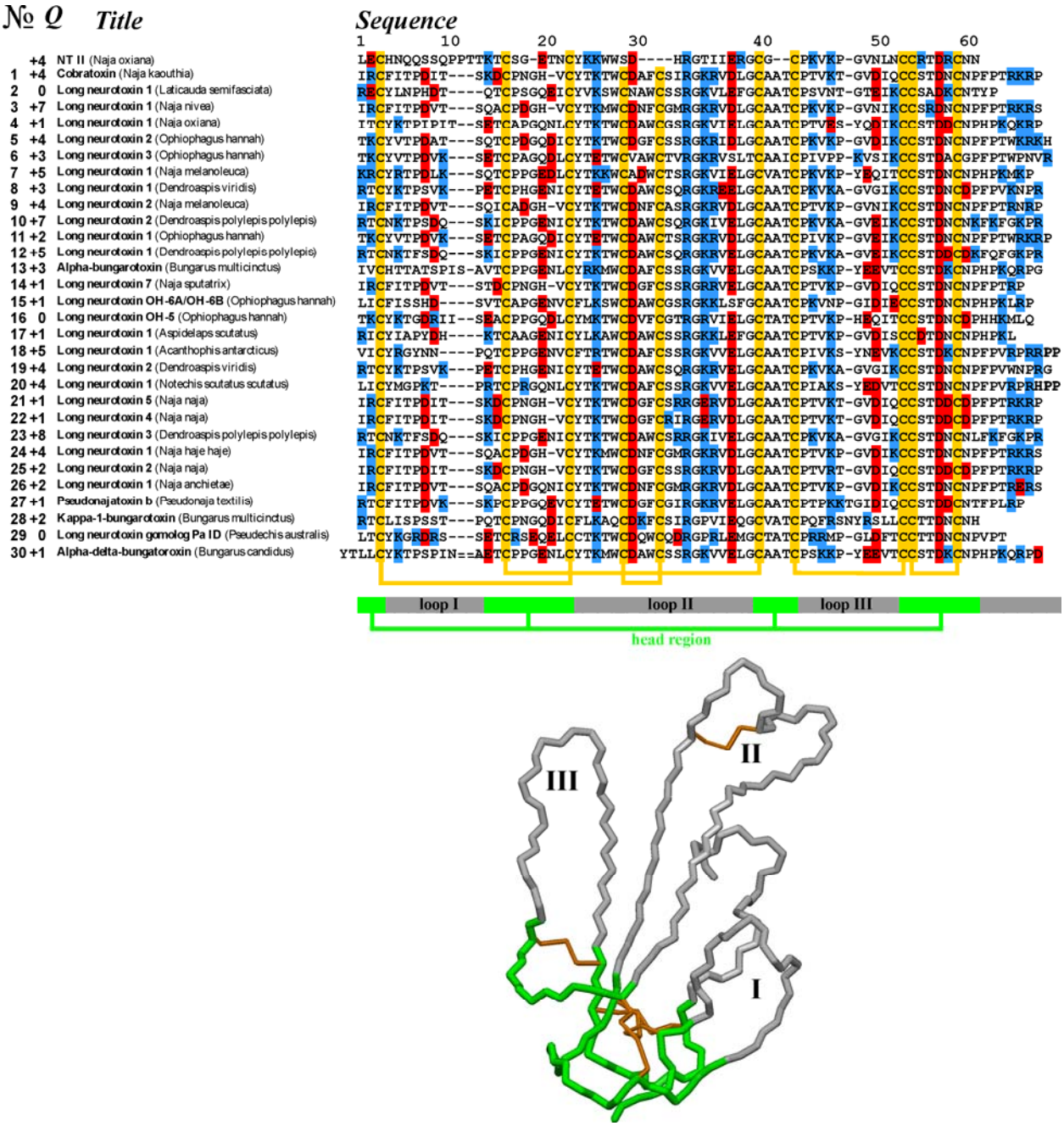

FIGURE S11 Sequence homology of short- and long-chain α-neurotoxins. The residue numbers are shown above the sequences and correspond to NTII. The toxins total charges Q are indicated for physiological pH 7.0. Cys residues, the residues with negatively (Asp and Glu) and positively (Arg and Lys) charged side chains are highlighted in *yellow*, *red,* and *blue*, respectively. At the bottom the structural elements S-S bonds, loops and head region of Cobratoxin are displayed in orange lines, green and gray boxes, respectively.

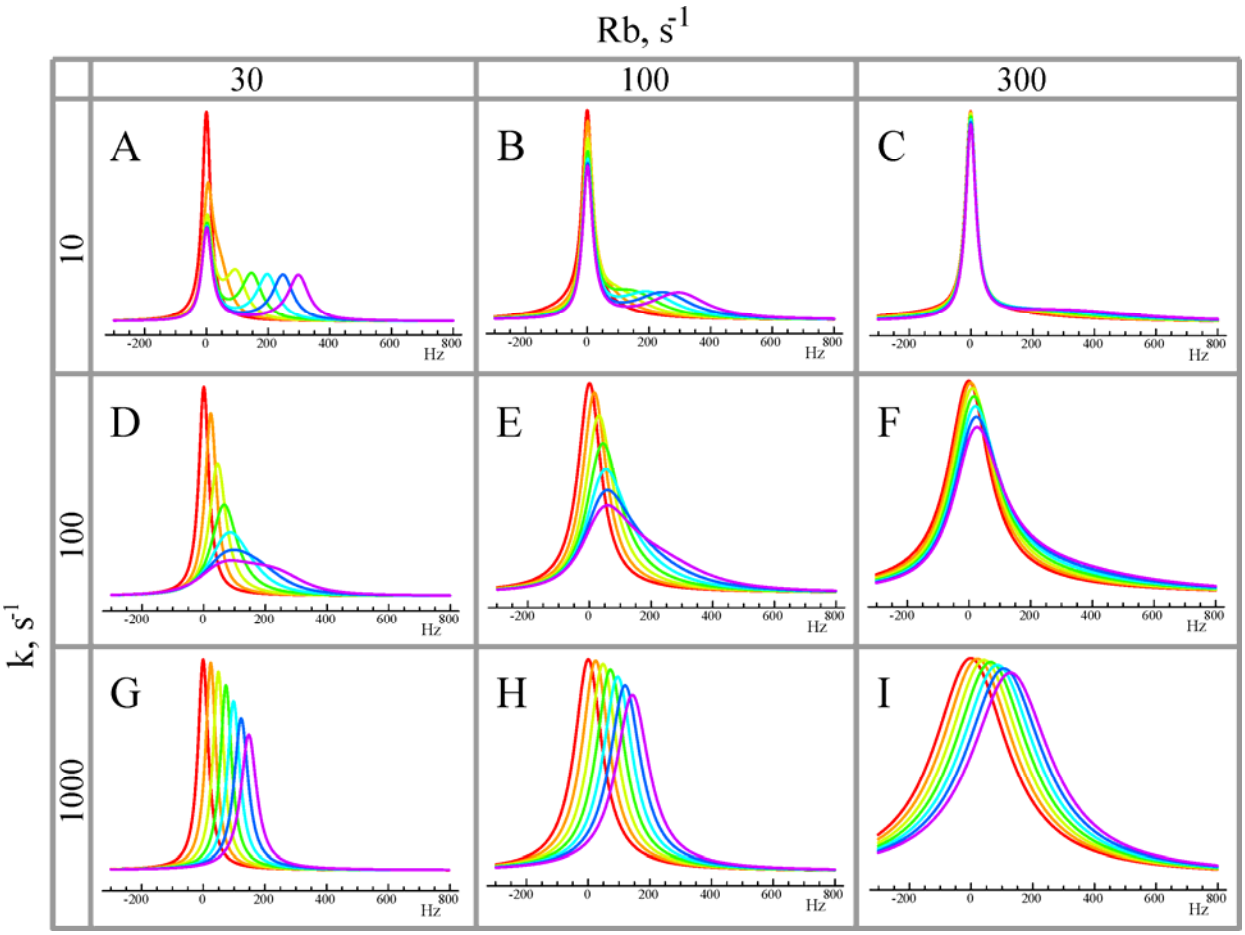

TABLE S1. Differential amplitude reduction effect as a function of the chemical shift difference between solution and membrane-bound states of NTII. Theoretical line shapes were simulated for chemical shift difference of $^{1}H^{N}$ signals of 0, 50, 100, 150, 200, 250, and 300 Hz (colored from red to violet, respectively) between free and membrane-bound states. In all cases, the fraction of free NTII is 0.5, R_f =10 c^{-1}, R_b and k values are presented in the table.

REFERENCES

1. Khechinashvili, N. N. and V. I. Tsetlin. 1984. Calorimetric study of heat denaturation of toxins. *Mol. Biol. (Mosk)* 18:786-791.
2. Polyansky, A. A., P. E. Volynsky, D. E. Nolde, A. S. Arseniev, and R. G. Efremov. 2005. Role of lipid charge in organization of water/lipid bilayer interface: insights via computer simulations. *J. Phys. Chem. B.* 109:15052-15059.
3. Berendsen, H. J. C., J. P. M. Postma, W. F. van Gunsteren, and J. Hermans. 1981. Interaction models for water in relation to protein hydration. *In* Intermolecular Forces. B. Pullman, editor. Reidel, Dordrecht. 331-342.
4. Darden, T., D. York, and L. Pedersen. 1993. Particle mesh Ewald: An N-log(N) method for Ewald sums in large systems. *J. Chem. Phys.* 98:10089-10092.
5. Berendsen, H. J. C., J. P. M. Postma, W. F. van Gunsteren, A. DiNola, and J. R. Haak. 1984. Molecular dynamics with coupling to an external bath. *J. Chem. Phys.* 81:3684-3690.
6. Matsuo, H., K. J. Walters, K. Teruya, T. Tanaka, G. T. Gassner, S. J. Lippard, Y. Kyogoku, and G. Wagner. 1999. Identification by NMR Spectroscopy of Residues at Contact Surfase in Large, Slowly Exchanging Macromolecular Complexes. *J. Am. Chem. Soc.* 121:9903-9904.
7. Walters, K. J., G. T. Gassner, S. J. Lippard, and G. Wagner. 1999. Structure of the soluble methane monooxygenase regulatory protein B. *Proc. Natl. Acad. Sci. U. S. A* 96:7877-7882.
8. Cavanagh, J., W. J. Fairbrother, A. G. Palmer III, M. Rance, and N. J. Skelton. 2007. Protein NMR Spectroscopy: Principles and Practice. ELSEVIER Academic Press, San Diego.
9. Dubovskii, P. V., D. V. Dementieva, E. V. Bocharov, Y. N. Utkin, and A. S. Arseniev. 2001. Membrane binding motif of the P-type cardiotoxin. *J. Mol. Biol.* 305:137-149.
10. Bychkova, V. E., A. E. Dujsekina, S. I. Klenin, E. I. Tiktopulo, V. N. Uversky, and O. B. Ptitsyn. 1996. Molten globule-like state of cytochrome c under conditions simulating those near the membrane surface. *Biochemistry* 35:6058-6063.
11. Dubinnyi, M. A., P. V. Dubovskii, I. Utkin, T. N. Simonova, L. I. Barsukov, and A. S. Arseniev. 2001. ESR study of the interaction of cytotoxin II with model membranes. *Bioorg. Khim.* 27:102-113.